Analysis of a singular stress field near the edge of joint using molecular dynamics

Hideo Koguchi[1,*], **Nobuyasu Suzuki**[1]

[1] Department of Mechanical Engineering, Nagaoka University of Technology, 940-2188, Japan
[2] Graduate School of Nagaoka University of Technology, 940-2188, Japan
* Corresponding author: koguchi@mech.nagaokaut.ac.jp

Abstract Recently, thin films with a nanometer thickness been used in electronic parts. When the size of material reduces to a nanometer, the area to volume ratio increases, then the mechanical property of surface or interface influences on mechanical behavior of bulk. Hence, it is very important to investigate the mechanical properties of interface and surface for the stress analysis in nano-scale materials. In the present paper, stress distribution near a wedge composed of several different materials is investigated using molecular dynamics (MD). The model used in the present analysis is a bonded joint of copper and gold, which is used in electronic parts. In the analysis, temperature of the model increases up to 5K for relaxation of the structure. A tensile load is applied in a radial direction along the outer surface of the model. The atomic stress distributions near the wedge tip in the joints and the angular function for the stress, which is derived from the theory of anisotropic elasticity, are compared. It can be found from the comparison that interface stress influences on the distribution of singular stress in the bulk and the intensity of singularity at the wedge tip.

Keywords Molecular dynamics, Singular stress, Interface, Joint, Stroh formalism

1. Introduction

Recently, thin films of nanometer thickness have been used in numerous electronic components in highly integrated devices, such as semiconductor devices. As the area-to-volume ratio increases in nanoscale structures, the physical properties of the surface or the interface affect the mechanical behavior near surface in bulk. Therefore, it is important to investigate the mechanical properties of the interface and the surface in the stress analysis of nanoscale materials. The molecular dynamics (MD) method can be used to evaluate the physical properties of materials in a nanometer scale by tracing individual atoms. Recently, Horiike et al.[1] investigated singular stress fields at the interfacial corner between dissimilar crystals using molecular statics (MS). In their analysis, a restricted displacement was applied to the outer surface in the joint model.
In the present paper, singular stress fields in joints composed of materials used in electronic devices are analyzed using MD. The atomic stress distribution near the edge of the joints is investigated under tensile loading in the radial direction. Incoherent interface and coherent interface models are used in the analysis. Through a comparison of the stress distributions in both models, the usefulness of the coherent interface model is demonstrated. It will be shown that if the atomic stress distribution before loading is subtracted from the stress distribution after loading, the stress distribution near the edge can be approximated by an equation based on the theory of anisotropic elasticity considering interface mechanical properties. Furthermore, the effect of wedge angles on the stress distribution will be investigated.

2. Singular stress analysis

From a standpoint in continuum mechanics, the stress distribution within singular stress fields near the edge of the interface in anisotropic joints can be expressed as

$$\sigma_{ij} = \sum_{m=1}^{n} K_{ij}^{m} f_{ij}^{m}(\theta) r^{-\lambda_m} \tag{1}$$

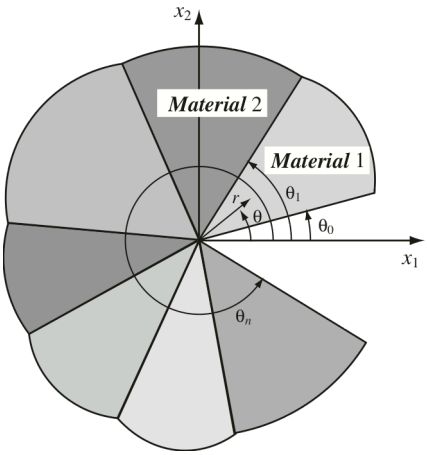

Figure 1. Multi-wedge model

where K_{ij}^{m} is the intensity of the singularity corresponding to the mth-order stress singularity, λ_m, r is the distance from a singular point [1], and $f_{ij}^{m}(\theta)$ is an angular function of stress σ_{ij}.

Koguchi derived an eigenequation with interface mechanics [2]. The eigenequation, **K,** is a 6×6 matrix composed of material properties and wedge angles and is expressed as follows:

$$\mathbf{K}=\begin{bmatrix}\mathbf{K}_1 & \mathbf{K}_2\\ \mathbf{K}_3 & \mathbf{K}_4\end{bmatrix}\begin{Bmatrix}\mathbf{p}^*\\ \mathbf{0}\end{Bmatrix}=\begin{bmatrix}\mathbf{G}_{1(1)} & \mathbf{G}_{1(0)}^{-1}\begin{bmatrix}\left\langle \hat{p}_{*1}^{1-\boldsymbol{\lambda}}(\boldsymbol{\theta}_1)\hat{p}_{*1}^{-1+\boldsymbol{\lambda}}(\boldsymbol{\theta}_0)\right\rangle & 0\\ 0 & \left\langle \hat{\bar{p}}_{*1}^{1-\boldsymbol{\lambda}}(\boldsymbol{\theta}_1)\hat{\bar{p}}_{*1}^{-1+\boldsymbol{\lambda}}(\boldsymbol{\theta}_0)\right\rangle\end{bmatrix}\end{bmatrix}$$
$$-\begin{bmatrix}\mathbf{A}_2 & \bar{\mathbf{A}}_2\\ \mathbf{B}_2 & \bar{\mathbf{B}}_2\end{bmatrix}\mathbf{G}_{2(2)}^{-1}\begin{bmatrix}\left\langle \hat{p}_{*2}^{1-\boldsymbol{\lambda}}(\boldsymbol{\theta}_1)\hat{p}_{*2}^{-1+\boldsymbol{\lambda}}(\boldsymbol{\theta}_2)\right\rangle & 0\\ 0 & \left\langle \hat{\bar{p}}_{*2}^{1-\boldsymbol{\lambda}}(\boldsymbol{\theta}_1)\hat{\bar{p}}_{*2}^{-1+\boldsymbol{\lambda}}(\boldsymbol{\theta}_2)\right\rangle\end{bmatrix}\begin{Bmatrix}\mathbf{p}^*\\ \mathbf{0}\end{Bmatrix}=\begin{Bmatrix}\mathbf{0}\\ \mathbf{0}\end{Bmatrix} \tag{2}$$

where $\mathbf{K}_i$ are 3×3 sub-matrices, **p*** represents the eigenvector of displacement, the angular brackets < > indicate a 3×3 diagonal matrix in which each component is changed according to its subscript, $\hat{p}_j(\theta)=\cos\theta+p_j\sin\theta$, λ is the singular order to be determined from the boundary conditions. Moreover, $\mathbf{A}_k$ and $\mathbf{B}_k$ are the matrices for material k given by the Stroh eigenvector, p_j is Stroh's eigenvalue, and $\bar{}$ denotes a complex conjugate [3], θ_i are the angles shown in Fig. 1., and $\mathbf{G}_{k(s)}$ is a 6×6 matrix that is defined as follows:

$$\mathbf{G}_{k(s)}=\Omega_k\begin{bmatrix}\mathbf{A}_k & \bar{\mathbf{A}}_k\\ \mathbf{B}_k & \bar{\mathbf{B}}_k\end{bmatrix}-\left(\mathbf{H}_{10s}-\frac{\mathbf{H}_{21s}}{\ell}\lambda\right)\Omega_k\begin{bmatrix}0 & 0\\ \mathbf{A}_k & \bar{\mathbf{A}}_k\end{bmatrix} \tag{3}$$

where

$$\Omega_k=\begin{bmatrix}\cos\theta & \sin\theta & 0\\ -\sin\theta & \cos\theta & 0\\ 0 & 0 & 1\end{bmatrix},\mathbf{H}_{10k}=\frac{1}{\ell}\begin{bmatrix}d_{1111i}^{k(a)} & 0 & d_{1131i}^{k(a)}\\ 0 & 0 & 0\\ d_{3111i}^{k(a)} & 0 & d_{3131i}^{k(a)}\end{bmatrix},\mathbf{H}_{21k}=\begin{bmatrix}d_{a1111i}^{k(a)} & 0 & d_{a1131i}^{k(a)}\\ 0 & \tau_{a11i}^{k(a)} & 0\\ d_{a1131i}^{k(a)} & 0 & d_{a3131i}^{k(a)}\end{bmatrix} \tag{4}$$

where ℓ is a representative length of stress field, $d_{\alpha\beta\gamma\delta i}$ are interface elastic constants, and $\tau_{\alpha\beta i}$ is interface stress.

The order of the singularity can be then obtained by setting to be zero the determinant of the coefficient matrix:

$$\left|\mathbf{K}_3\right|=0 \tag{5}$$

The eigenvalue, λ, obtained from Eq. (5) exists infinitely. However, the stress field at the tip in an anisotropic elastic composite wedge is expressed primarily in terms of the stress singularity. Displacements in the singular stress field are definite. Hence, $0 < \mathrm{Re}(\lambda) < 1$.

If the angular function for the displacement is expressed by $m_k^j(\theta)$, the angular function $f_k^j(\theta)$ for

stress is given by

$$\left\{ \begin{array}{c} \mathbf{m}_k \\ \mathbf{f}_k \end{array} \right\} = \left[\begin{array}{cc} \mathbf{A}_k & \bar{\mathbf{A}}_k \\ \mathbf{B}_k & \bar{\mathbf{B}}_k \end{array} \right] \mathbf{G}_{k(j)} \left[\begin{array}{cc} \left\langle \hat{p}_{*k}^{1-\lambda}(\theta) \hat{p}_{*k}^{-1+\lambda}(\theta_2) \right\rangle & 0 \\ 0 & \left\langle \hat{\bar{p}}_{*k}^{1-\lambda}(\theta) \hat{\bar{p}}_{*k}^{-1+\lambda}(\theta_2) \right\rangle \end{array} \right] \left\{ \begin{array}{c} \mathbf{p}^* \\ \mathbf{0} \end{array} \right\} \tag{6}$$

where j=0 for k=1 and j=2 for k=2.Here, the stress function is expressed as $\boldsymbol{\phi}^{(k)} = K_m r^{\lambda_m} \mathbf{f}^k(\theta)$.

3. Molecular dynamics

3.1. GEAM potensial

The molecular dynamics method is used for rearranging atomic structures near surfaces and interfaces, and the distribution of atomic stress near the tip of the wedge is calculated using the GEAM potential, which can be used to adequately express the potential for joint structures composed of anisotropic materials. The GEAM potential is composed of many-body and two-body potentials, which covers multi-component systems [4, 5].
The GEAM potential E is defined as

$$E_{tot} = \sum_{\alpha} \left\{ F_{\alpha}\left(\rho^{\alpha}\right) + \frac{1}{2} \sum_{\beta(\neq\alpha)} V_{\alpha\beta}\left(r^{\alpha\beta}\right) \right\} \tag{7}$$

where the embedding function F_{α}, which gives the potential energy arising from embedding a particular atom having electron density ρ^{α} at the site α, and $V_{\alpha\beta}$ is the pair interaction between atoms α and β, the separation of which is given by $r^{\alpha\beta}$. In the present analysis, Cu and Au are used for a joint model. The two-body cross potential $V^{\text{Cu-Au}}(r)$ between Au and Cu is constructed as

$$V^{Cu-Au}(r) = \frac{1}{2}\left[\frac{g^{Cu}(r)}{g^{Au}(r)} V^{Au-Au}(r) + \frac{g^{Au}(r)}{g^{Cu}(r)} V^{Cu-Cu}(r) \right] \tag{8}$$

where $g^{A}(r)$ and $V^{A\text{-}A}(r)$ are the functions of $g(r)$ and $V(r)$ for material A, respectively
The atomic stress is given by

$$\sigma_{ij}^{\alpha} = \frac{1}{\Omega^{\alpha}} \frac{\partial E_{\alpha}}{\partial \varepsilon_{ij}} \tag{9}$$

where Ω^{α} is Voronoi volume of atom α, and ε_{ij} is the bulk strain.

3.2. Models in MD analysis

The material combination of (Material 1, Material 2) = (Cu, Au) is employed. In modeling the joint, a prior calculation for determining the gap at the interface between Cu and Au was carried out. In the calculation, a bicrystalline model with a constant thickness was used. Coherent and incoherent bicrystalline interface models composing of fcc crystal cells with dimensions $10c \times 10c \times 14c$ (the lower region) and $10c \times 10c \times 10c$ (the upper region) along the cubic axes of the conventional unit cell [100], [010] and [001], respectively are considered. c is the lattice constant of the crystal. Here, the coherent interface model has an average lattice parameter of material 1 and material 2. The potential parameter in both materials is modified due to the change of the lattice parameter. Bicrystal (100) plane is the interface plane. Periodic boundary conditions are imposed along the [100] and [010] directions, and the top and bottom planes normal to [001] direction are free. The lattice constant c is 0.3615nm for Cu and 0.4086nm for Au. The gap between Cu and Au is determined for minimizing the interface energy. In the analysis, temperature in the model is varied for achieving the relaxation of atomic structures, i.e., temperature is increased up to 5K until 1000

steps, is kept at 5K until 7000 steps, is decreased down to 0K until 9000 steps, and is kept at 0K until 10000 steps. Time step in the MD calculation is 50fs.

Figure 2 shows a wedge model consisting of two different materials. In the model, radius a is 7 nm, and the thickness is 2 nm. The total number of atoms is from 13,000 to 15,000. Boundaries Γ_1 and Γ_2 are free surfaces, and the periodic boundary condition is applied in the z-direction. An external traction F of 100 MPa is applied in the normal direction of the outer surface Γ_o. The crystal plane on the interface is (001). The wedge angle ω is varied from 90º to 170°, and a precise analysis of the result obtained at ω= 170º using models with coherent and incoherent interfaces is performed. A joint model of ω=170º with the incoherent interface is shown in Fig.3.

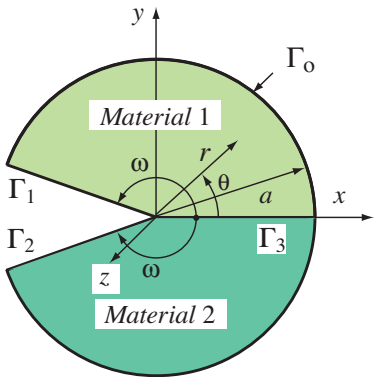

Figure 2. Wedge model for analysis

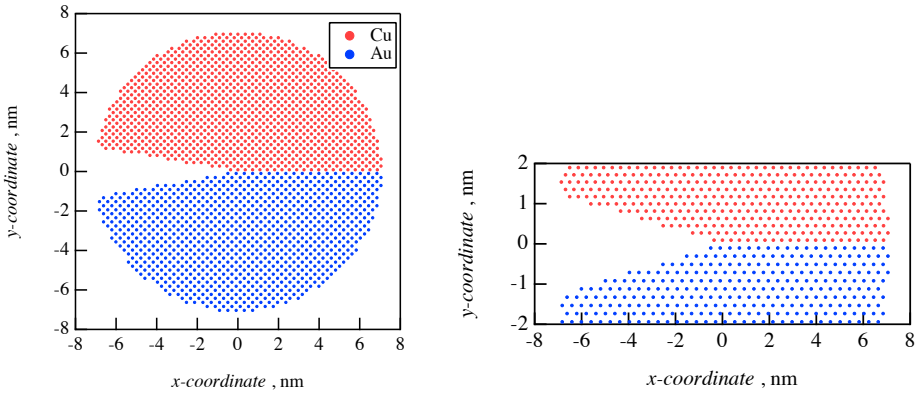

(a) A joint model with ω=170º in MD (b) Enlargement along the interface

Figure 3. MD model for the joint (red symbol : Cu, blue symbol : Au)

4. Results of anaysis

4.1. Results for an incoherent interface

A model with an incoherent interface is firstly analyzed. A distribution map of the stress σ_{yy} in the x-y plane is shown in Fig. 4. The plane is selected so that the misfit of the z-direction is the smallest. The stress is calculated using eq.(8) in which the Voronoi volume is involved. Moreover, the distribution of stress σ_{yy} along the interface is shown in Fig. 5. The stress distribution fluctuates along the interface since the Voronoi volume may be vary. The stress near the interface varies periodically, as shown in Fig. 4. This is attributed to the influence of lattice misfit. The period of the

stress variation is approximately 3 nm and agrees with the distance between the smallest lattice misfit in the x-direction. This stress variation does not exist in the model with a coherent interface.
In order to investigate the influence of interface and surface stresses on the stress distribution near the wedge, an initial stress before loading is subtracted from the distribution shown in Fig. 5. The stress distribution along the interface is shown in Fig. 6. It is found that the difference in stress between Au and Cu becomes small, and the stress near the wedge subsequently becomes large.

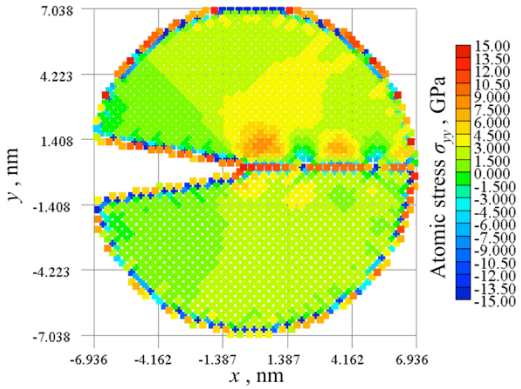

Figure 4. Stress distribution, σ_{yy}, in incoherent model

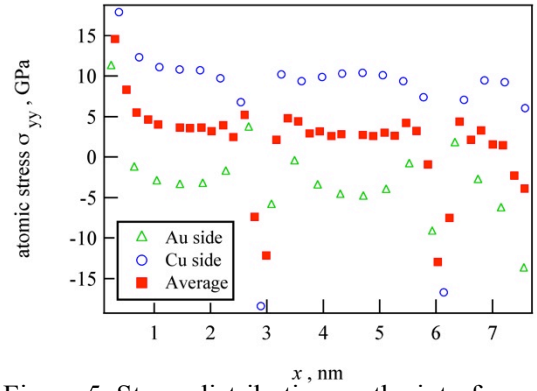

Figure 5. Stress distribution on the interface, σ_{yy} (incoherent interface model)

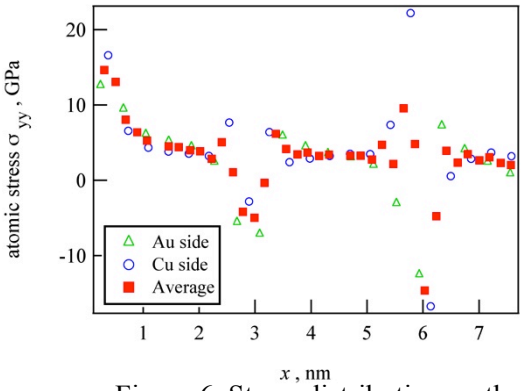

Figure 6. Stress distribution on the interface, σ_{yy}, after subtracting initial stress (incoherent interface model)

4.2. Results for a coherent interface

Next, the model with a coherent interface is analyzed. The lattice length in the model is the average of the lattice lengths of Au and Cu. The potential parameters r_e of Au and Cu in the model are changed due to the change in the lattice length. A distribution map of the stress σ_{yy} in the x-y plane is shown in Fig. 7. The distributions of stress σ_{yy} for incoherent and coherent interfaces along the interface are shown in Fig. 8. The stress in the coherent model distributes smoothly, except near the edge of the interface.
As shown in Fig. 7, the stress in the direction of about 45° from the interface is larger, and the contour of the stress distribution is a fan shape. The stress in Cu (the upper material) is larger than that in Au. The atomic stress along the interface is slightly larger than that in other locations. The stresses on Γ_1, Γ_2, and Γ_0 in the model are large due to the influence of the surface or the interface. In Fig. 8, the stress (blue open circle) decreases slightly at x = 0.5 nm. The same tendency can be seen in the results of the surface stress analysis [6]. This is due to the influence of surface effect.

In order to investigate the influence of interface and surface stresses on the stress distribution near the wedge, the initial stress before loading is subtracted from the distribution shown in Fig. 8. The results for the stress distribution are shown in Fig. 10. The difference in stress between the Au and Cu regions decreases, and the stress near the wedge becomes large. The distribution of stress σ_{yy} on $r = 4$ nm is shown in Fig. 9. The stress distribution is disturbed near the interface. This is due to the interface stress effect. A comparison of the results for the coherent interface and the incoherent interface is shown in Fig. 10. Figure 10 shows the stress distribution obtained after subtracting the initial stress from the distribution shown in Fig. 8. When the initial stress is subtracted, the stress distribution on the incoherent interface approaches to that on the coherent interface.

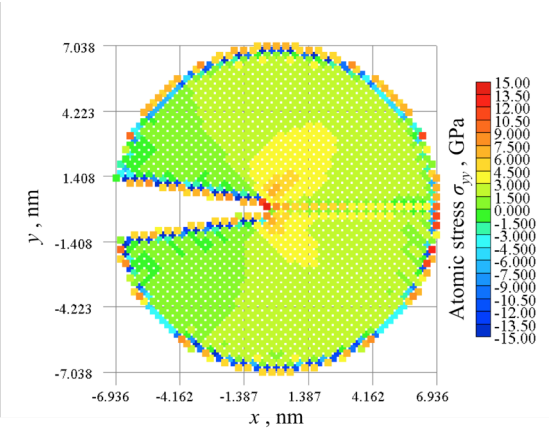

Figure 7. Stress distribution, σ_{yy}, in coherent model

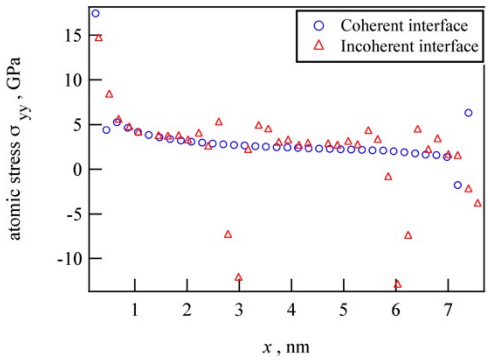

Figure 8. Stress distribution on the interface, σ_{yy}, including the initial stress

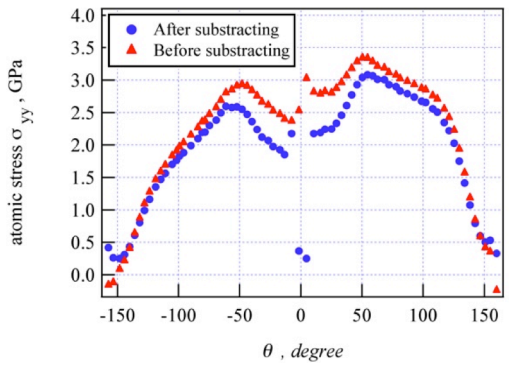

Figure 9. Stress distribution on a circle of radius 4 nm

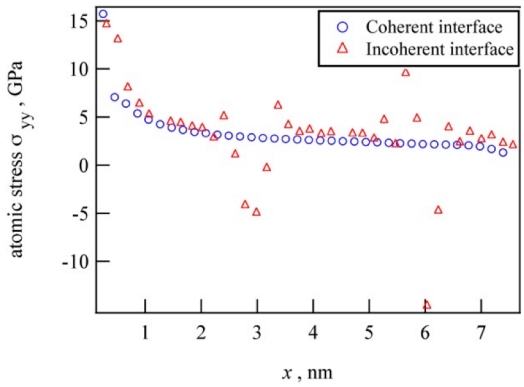

Figure 10. Stress distribution on the interface, σ_{yy}, after subtracting the initial stress

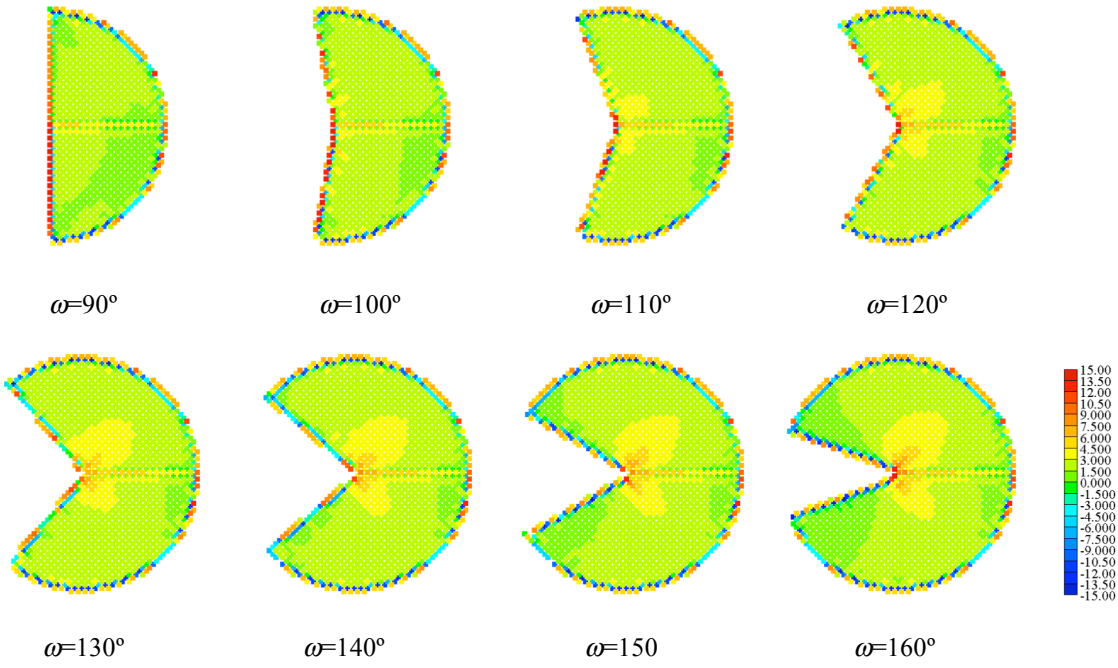

Figure 11. Contour map of stress, σ_{yy}, in coherent interface model with various wedge angles (Before subtracting the initial stress)

4.3. Influence of wedge angle on the stress distribution

Here, the influence of the wedge angle, ω, on the stress distribution σ_{yy} is investigated. The angle ω is varied from 90° to 170° at 10° intervals. A surface traction of 100 MPa is applied to the outer surface Γ_o. A coherent interface model is used for the analysis. The results of the analysis are shown in Fig. 11. A small stress concentration appears in the model with ω= 90°. As the wedge angle ω increases, the stress concentration increases. In particular, as shown in these figures, the region of large stress extends in the directions of θ= 65° and -70°. The distributions of atomic stress σ_{yy} for various wedge angles ω along the interface are shown in Fig. 12. Figures 12(a) and 12(b) show the stress distributions including the initial stress and subtracting the initial stress, respectively. These stresses are the average values for the nearest atom in both regions. The stress σ_{yy} increases with the wedge angle ω.

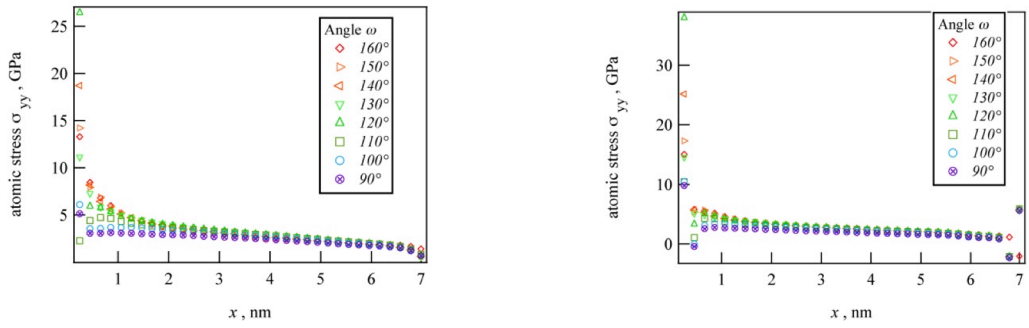

(a) Before subtraction (b) After subtraction

Figure 12. Distribution of atomic stress σ_{yy} along the interface

4.4. Comparison of the MD results for stress singularity and angular function

The order of stress singularity λ is obtained for various angle ω using Eq. (5). The angle ω is varied from 90° to 180°. The value of λ is shown in Fig. 13. A complex value of λ appears in the range $174° < \omega \leq 180°$. In the case of $\omega = 180°$, λ is $0.5 \pm i\varepsilon$ (where ε is a constant that depends on the material combination: 0.0042(Cu-Au)). This case corresponds to a notch.
Figure 14 shows both log plots of the data shown in Fig. 12. Figures 14(a) and 14(b) are stress distributions including and subtracting the initial stress, respectively. As shown in these figures, the stress distribution after subtracting the initial stress is straighter than that before subtracting the initial stress. Next, the results for $\omega = 170°$ are precisely investigated. Figure 13 shows that the imaginary part of λ for $\omega = 170°$ does not exist and that three roots exist corresponding to $\lambda_{\mathrm{I}} = 0.499$, $\lambda_{\mathrm{II}} = 0.462$, and $\lambda_{\mathrm{III}} = 0.461$. The angular functions are continuous at the interface, and f^{II} and f^{III} are approximately 0 around $\theta = 0°$ and at the free surface ($\theta = \pm 170°$). Hence, the stress distribution along the interface may be expressed by a power-law with an index of -0.499. The stress distributions shown in Figs. 8 and 10 are then compared with the stress distributions approximated using $\sigma_{yy} = K_{yy} r^{-0.499}$. Here, r is used in place of x.

Both log plots for σ_{yy} in the incoherent model are shown in Fig. 15. Figure 15(a) represents the stress distribution before subtracting the initial stress due to surface stress. Figure 15(b) demonstrates the stress distribution after subtracting the initial stress. The blue line in these figures indicates the approximated stress distribution using Eq. (9). As shown in Fig. 15(b), the atomic stress σ_{yy} with the initial stress subtracted agrees fairly well with the approximated line in 0.6 nm < r < 2 nm. However, the atomic stress increases near the tip and is larger than the approximated line given by the power-law that is derived from the theory of anisotropic elasticity. This might be due to a variation in surface stress near the tip. Log plots of atomic stress σ_{yy} in the coherent model are shown in Fig. 16. Figure 16(a) shows the distribution of atomic stress σ_{yy} corresponding to Fig. 15(a). The blue line indicates the plot of the same line shown in Fig. 15. The blue line does not agree with the atomic stress shown in Fig. 16(a). The stress distribution with the initial stress subtracted agrees fairly well with the blue line, as shown in Fig. 16(b). However, the atomic stress σ_{yy} becomes larger than the value estimated from the theory of anisotropic elasticity near the tip. Here, the order of stress singularity is determined as a function of distance along the interface using eqs.(2)-(5). The interface stress and interface elastic moduli are obtained as functions of the distance of the wedge tip along the interface. These relationships are used for solving eq.(5). The order of stress singularity is plotted against the distance as shown in Fig. 17. The plotted values are approximated using the power law function of the distance r as $\lambda_1(r) = 0.496 + 0.00114\left(r/\ell\right)^{-4.45}$. Here, $\ell = 1$nm. Then, the distribution of atomic stress along the interface is presented in Fig. 18. It is found that the atomic stress can be expressed by the equation of $4.8r^{-\lambda_1(r)}$ considering the interface stress and elasticity.

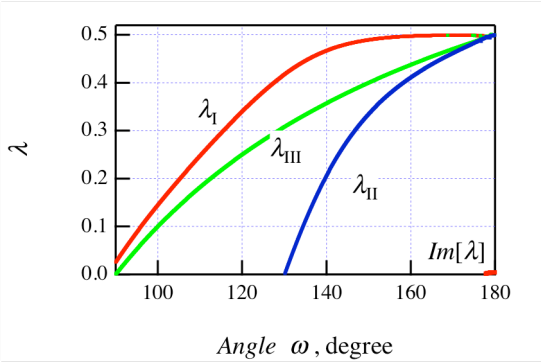

Figure 13. Order of stress singularity λ against the angle ω

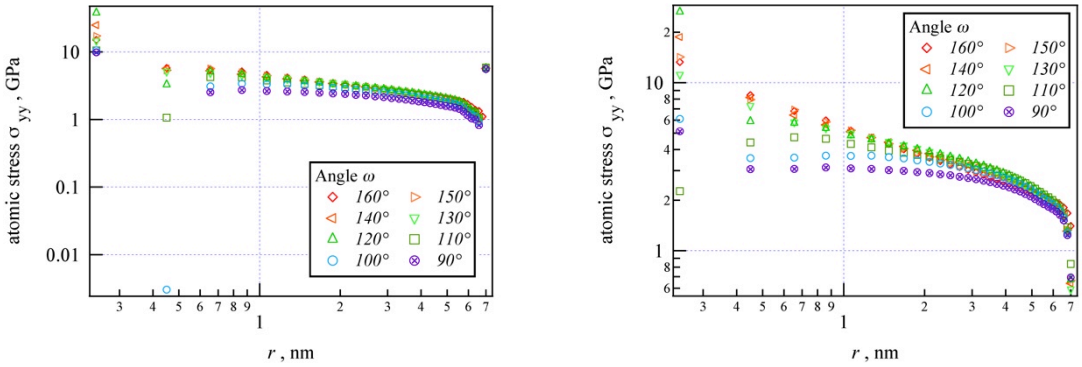

(a) Before subtraction (b) After subtraction

Figure 14. Both log plots of the atomic stress σ_{yy} along the interface

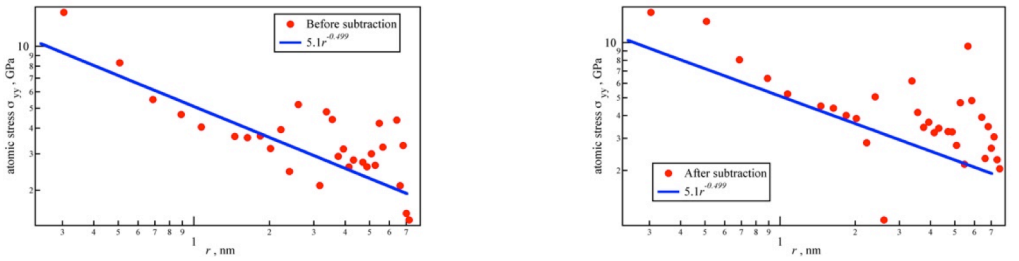

(a) Before subtracting the initial stress (b) After subtracting the initial stress

Figure 15. Stress distribution along the interface in the incoherent model

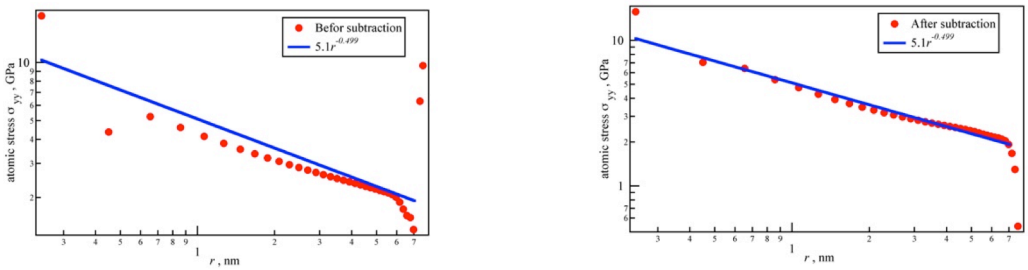

(a) Before subtracting the initial stress (b) After subtracting the initial stress

Figure 16. Distribution of stress, σ_{yy}, on the interface in the coherent interface model

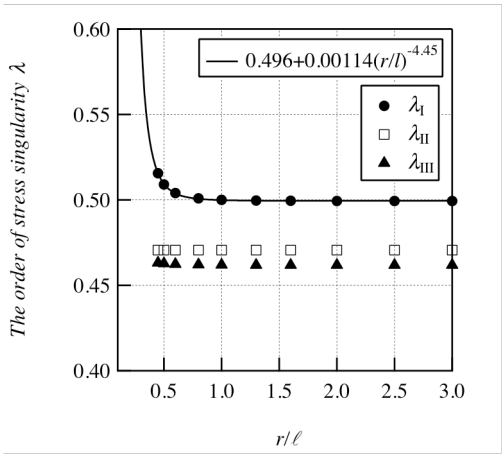

Figure 17. A variation of the order of stress the singularity

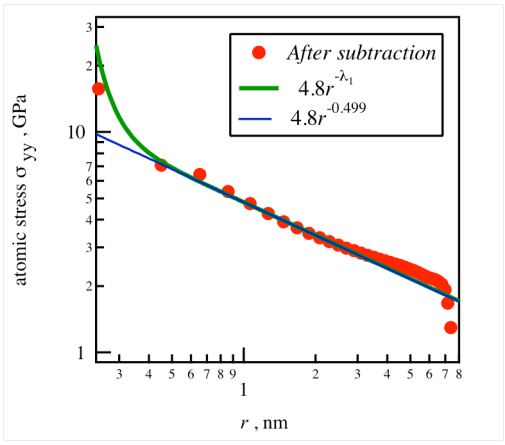

Figure 18. Distribution of stress σ_{yy} along interface

5. Conclusions

In the present paper, the stress distributions in incoherent and coherent wedge models were analyzed using MD, in which the GEAM potential was used. The stress distributions in both models were compared, and the usefulness of coherent model was demonstrated. The coherent model is applicable for analyzing the stress singular field by subtracting the initial stress from the stress distribution after loading. The stress distribution near the edge tip of the interface in MD can be expressed using the anisotropic theory of elasticity considering the interface properties.

Acknowledgements

The present research was supported in part by a Grant-in-Aid for Scientific Research (B) (No. 2136051) from the Japan Society for the Promotion of Science.

References

[1] Horike K., Ikeda T., Matumoto R. and Noriyuki N., Stress Singularity Analysis at an Interfacial Corner between Dissimilar Crystals and Evaluation of Mixed Modes Fracture Criteria Using Molecular Statics, *Journal of the Society of Materials Science*, Vol. 59, No. 12, (2010), pp.908-915.

[2] Koguchi H., Analysis for Stress Singular Fields near a Wedge Corner in 2D Joints Considering Interface Elasticity, ASME 2012 International Mechanical Engineering Congress & Exposition, 2012.

[3] Ting T. C. T., Anisotropic Elasticity: Theory and Applications, Oxford University Press, (1996), pp.134-263.

[4] Wadley H.N.G., Zhou X., Johnson R.A. and Neurock M., Mechanisms, models and methods of vapor deposition, *Progress in Materials Science,* 46, Issue 3-4(2001), pp.329-377.

[5] Zhou X. W, Wadley H. N. G. and Johnson R. A, Atomic Scale Structure of Sputtered Metal Multilayer, *Acta Materialia*, 49, (2001), pp.4005-4015.

Appendix

The embedding function is defined as

$$F(\rho)=\begin{cases}\sum_{i=0}^{3}F_{ni}\left(\frac{\rho}{\rho_n}-1\right)^i & (\rho<\rho_n,\rho_n=0.85\rho)\\ \sum_{i=0}^{3}F_i\left(\frac{\rho}{\rho_e}-1\right)^i & (\rho<\rho_e,\rho_e=1.15\rho)\\ F_e\left[1-\ln\left(\frac{\rho}{\rho_e}\right)^n\right]\left(\frac{\rho}{\rho_e}\right)^n\end{cases} \tag{10}$$

$$V(r)=\frac{A\exp\left[-\alpha\left(\frac{r}{r_e}-1\right)\right]}{1+\left(\frac{r}{r_e}-\kappa\right)^{20}}+\frac{B\exp\left[-\beta\left(\frac{r}{r_e}-1\right)\right]}{1+\left(\frac{r}{r_e}-\lambda\right)^{20}} \tag{11}$$

$$\rho=\sum_{\beta(\neq\alpha)}g(r) \tag{12}$$

$$g(r)=\frac{g_e\exp\left[-\beta\left(\frac{r}{r_e}-1\right)\right]}{1+\left(\frac{r}{r_e}-\lambda\right)^{20}} \tag{13}$$

The two-body cross potential $V^{\text{Cu-Au}}(r)$ between Au and Cu is constructed as

$$V^{Cu-Au}(r)=\frac{1}{2}\left[\frac{g^{Cu}(r)}{g^{Au}(r)}V^{Au-Au}(r)+\frac{g^{Au}(r)}{g^{Cu}(r)}V^{Cu-Cu}(r)\right] \tag{14}$$

where $g^A(r)$ and $V^{A\text{-}A}(r)$ are the functions of $g(r)$ and $V(r)$ for material A, respectively, g_e, r_e, ρ_e, α, β, A, B, κ, λ, F_{ni}, F_i, η, and F_e are potential parameters[4],[5].

Table 1 Values of potential functions

	Au	Cu		Au	Cu
r_e	2.88503	2.556162	F_{n0}	−2.937772	−2.170269
g_e	1.529021	1.554485	F_{n1}	−0.500288	−0.263788
ρ_e	19.991632	21.175871	F_{n2}	1.601954	1.088878
ρ_n	19.991509	21.175395	F_{n3}	−0.83553	−0.817603
ι	9.516052	8.12762	F_0	−2.98	−2.19
χ	5.075228	4.334731	F_1	0	0
B	0.229762	0.39662	F_2	1.706587	0.56183
κ	0.356666	0.548085	F_3	−1.134778	−2.100595
λ	0.35657	0.308782	η	1.021095	0.31049
λ_n	0.748798	0.756515	F_e	−2.978815	−2.186568